

Neural Pushforward Samplers for the Fokker–Planck Equation on Embedded Riemannian Manifolds

Andrew Qing He* Wei Cai†

March 2026

Abstract

We extend the Weak Adversarial Neural Pushforward Method (WANPF) to the Fokker–Planck equation posed on a compact, smoothly embedded Riemannian manifold $M \hookrightarrow \mathbb{R}^n$. The key observation is that the weak formulation of the Fokker–Planck equation, together with the ambient-space representation of the Laplace–Beltrami operator via the tangential projection $P(x)$ and the mean-curvature vector $H(x)$, permits all integrals to be evaluated as expectations over samples lying on M , using test functions defined globally on \mathbb{R}^n . A neural pushforward map F_{ϑ} is constrained to map the support of a base distribution into M at all times through a manifold retraction Π_M , so that probability conservation and manifold membership are enforced by construction. Adversarial ambient plane-wave test functions are chosen, and their Laplace–Beltrami operators are derived in closed form, enabling autodiff-free, mesh-free training. We present both a steady-state and a time-dependent formulation, derive explicit Laplace–Beltrami formulae for the sphere S^{n-1} and the flat torus \mathbb{T}^n , and demonstrate the method numerically on a double-well steady-state Fokker–Planck equation on S^2 . The trained generator concentrates mass near the two potential minima at $(\pm 1, 0, 0)$, consistent with the Boltzmann distribution of the underlying Langevin dynamics.

Keywords: Fokker–Planck equation, Riemannian manifold, neural pushforward map, weak adversarial network, Laplace–Beltrami operator, plane-wave test functions, steady-state distribution, sphere.

MSC 2020: 65N75; 68T07; 58J65; 35Q84.

Contents

1	Introduction	3
2	Setting and Notation	4

*Department of Mathematics, Southern Methodist University, Dallas, TX 75275. andrewho@smu.edu

†Department of Mathematics, Southern Methodist University, Dallas, TX 75275. cai@smu.edu

3	Steady-State WANPF on a Manifold	4
3.1	Strong Formulation	4
3.2	Weak Formulation	5
3.3	Pushforward Architecture and Adversarial Loss	5
4	Ambient Plane-Wave Test Functions	5
4.1	Definition	5
4.2	Laplace–Beltrami Action on Plane Waves	6
5	Manifold-Constrained Pushforward Architecture	6
5.1	Retraction-Based Generator	6
5.2	Network Specification	7
6	Time-Dependent WANPF on a Manifold	7
6.1	Weak Formulation	7
6.2	Monte Carlo Estimators	7
6.3	Adversarial Training Objective	8
7	Explicit Formulae for Key Manifolds	8
7.1	The Unit Sphere $S^{n-1} \subset \mathbb{R}^n$	8
7.2	The Flat Torus $\mathbb{T}^n \subset \mathbb{R}^{2n}$	9
8	Numerical Experiment: Double-Well FPE on S^2	9
8.1	Problem Setup	9
8.2	Ambient Gradient and Drift	9
8.3	Architecture and Training	9
8.4	Results	10
9	Discussion	10
9.1	Advantages of the Manifold Formulation	10
9.2	Connection to Geometric Measure Theory	11
9.3	Extension to Non-Isotropic Diffusion	11
9.4	Supplementing with Spherical Harmonics	12
9.5	Future Directions	12
10	Conclusion	13

1 Introduction

A wide class of stochastic differential equations (SDEs) arising in molecular dynamics, robotics, directional statistics, and climate science evolve not in flat Euclidean space but on a constraint surface: a sphere, a torus, a Stiefel manifold, or more generally a smooth Riemannian manifold (M, g) [2–4]. The natural companion PDE governing the time evolution of the probability density is the Fokker–Planck equation (FPE) on (M, g) ,

$$\frac{\partial \rho}{\partial t} = \frac{\sigma^2}{2} \Delta_g \rho - \operatorname{div}_g(\rho \mathbf{b}), \quad (1)$$

where Δ_g is the Laplace–Beltrami operator, \mathbf{b} is a smooth tangential drift, and $\sigma > 0$ is the diffusion coefficient.

Solving (1) numerically is challenging for two independent reasons. First, classical finite-difference or finite-element methods require an explicit triangulation of M , which becomes prohibitively expensive in moderate to high dimension. Second, even for simple manifolds such as S^{n-1} with $n \geq 4$, the curse of dimensionality prevents grid-based methods from being practically viable.

Recent work has addressed these difficulties for flat-space FPEs by representing the solution *distribution* rather than a pointwise density, through a neural pushforward map trained with a weak adversarial objective [1]. In that approach, a generator network F_θ pushes a simple base distribution forward to approximate the FPE solution at any queried time, with training guided by a three-term Monte Carlo weak formulation that avoids any spatial mesh.

The present paper extends this Weak Adversarial Neural Pushforward Method (WANPF) to the Riemannian setting. The extension rests on two structural observations.

1. **Non-invertibility is an asset.** The pushforward map $F_\theta : \mathbb{R}^d \rightarrow M$ need not be invertible, and the base dimension d need not equal $\dim M$. This is impossible for normalizing-flow or change-of-variables methods, and it is what allows WANPF to use a higher-dimensional noise space for greater representational capacity.
2. **Weak integrals become pointwise expectations.** After integrating by parts, every spatial operator in the weak form acts on the test function rather than on ρ . The Laplace–Beltrami operator applied to an ambient plane-wave test function can be computed in closed form at each sample, using only the tangential projection $P(x) = I - xx^\top$ (for the sphere) and the mean-curvature vector $H(x)$. No automatic differentiation through the intrinsic geometry is required.

The result is a fully mesh-free, chart-free, and Jacobian-free training procedure. The generator’s samples are constrained to M via a manifold retraction Π_M (e.g., normalization to the unit sphere), and the initial condition is satisfied automatically by the pushforward architecture.

Contributions.

- A complete steady-state WANPF formulation for the manifold FPE, including the adversarial min-max loss and its Monte Carlo estimator (Section 3).

- A time-dependent WANPF formulation with a three-term weak form (Section 6), matching the flat-space structure of [1].
- Closed-form Laplace–Beltrami plane-wave formulae for S^{n-1} and \mathbb{T}^n (Sections 4–7).
- Numerical experiments on the double-well FPE on S^2 , demonstrating that the trained generator correctly concentrates mass near the two Boltzmann minima (Section 8).

Organization. Section 2 introduces the manifold FPE and fixes notation. Section 3 derives the steady-state WANPF. Section 4 derives the ambient plane-wave Laplace–Beltrami formulae. Section 5 specifies the pushforward architecture. Section 6 derives the time-dependent WANPF. Section 7 records explicit formulae for the sphere and torus. Section 8 presents the numerical experiments. Section 9 discusses extensions.

2 Setting and Notation

Throughout, (M, g) is a smooth, compact, connected Riemannian manifold without boundary, isometrically embedded in \mathbb{R}^n . Compactness ensures global probability conservation and the absence of spatial boundary conditions. Let $m = \dim M \leq n - 1$.

For any $x \in M$, let $T_x M \subset \mathbb{R}^n$ denote the tangent space of M at x . We write $P(x) \in \mathbb{R}^{n \times n}$ for the orthogonal projection onto $T_x M$, so $P(x)^2 = P(x)$, $P(x)^\top = P(x)$, and $P(x)v$ is the tangential component of any ambient vector $v \in \mathbb{R}^n$.

The *mean-curvature vector* $H(x) \in \mathbb{R}^n$ of the embedding is

$$H(x) = \text{tr}(\partial_i P(x)), \quad (2)$$

where the trace is over the n coordinate directions. For a smooth ambient function $f : \mathbb{R}^n \rightarrow \mathbb{R}$, the intrinsic gradient and Laplace–Beltrami operator on M are:

$$\nabla_g f(x) = P(x) \nabla f(x), \quad (3)$$

$$\Delta_g f(x) = \nabla^2 f(x) : P(x) - \nabla f(x) \cdot H(x), \quad (4)$$

where ∇f and $\nabla^2 f$ are the Euclidean gradient and Hessian of the ambient extension of f , and $A : B = \text{tr}(A^\top B)$. For flat subspaces, $H = 0$ and (4) reduces to the standard Laplacian restricted to the subspace.

The drift \mathbf{b} is a smooth tangential vector field on M , and in applications derived from a potential $V : \mathbb{R}^n \rightarrow \mathbb{R}$ it takes the form $\mathbf{b}(x) = -P(x)\nabla V(x)$, which is automatically tangential.

3 Steady-State WANPF on a Manifold

3.1 Strong Formulation

The steady-state FPE seeks a probability measure ρ on M satisfying:

$$\frac{\sigma^2}{2} \Delta_g \rho - \text{div}_g(\rho \mathbf{b}) = 0, \quad \int_M \rho \, \text{dVol}_g = 1, \quad \rho \geq 0. \quad (5)$$

On a compact manifold without boundary the Fredholm alternative guarantees the existence and, under mild irreducibility conditions on \mathbf{b} , the uniqueness of an invariant measure. When $\mathbf{b} = -\nabla_g V$ for a potential V , the unique invariant measure is the Gibbs distribution $\rho_\infty \propto e^{-2V/\sigma^2}$.

3.2 Weak Formulation

Multiplying (5) by a test function $f \in C^\infty(M)$, integrating over M against $d\text{Vol}_g$, and integrating by parts (boundary terms vanish by compactness) gives:

$$\int_M \rho(x) \mathcal{L}_{\text{ss}} f(x) d\text{Vol}_g = 0, \quad (6)$$

where the *backward Kolmogorov operator* for the steady-state problem is:

$$\mathcal{L}_{\text{ss}} f := \frac{\sigma^2}{2} \Delta_g f + \langle \mathbf{b}, \nabla_g f \rangle_g. \quad (7)$$

Equation (6) is an expectation condition:

$$\mathbb{E}_{\mathbf{x} \sim \rho}[\mathcal{L}_{\text{ss}} f(\mathbf{x})] = 0 \quad \forall \text{ admissible } f. \quad (8)$$

3.3 Pushforward Architecture and Adversarial Loss

For the steady-state problem the pushforward map has no temporal argument:

$$F_\vartheta : \mathbb{R}^d \rightarrow M, \quad F_\vartheta(\mathbf{r}) = \Pi_M(\tilde{F}_\vartheta(\mathbf{r})), \quad (9)$$

where $\tilde{F}_\vartheta : \mathbb{R}^d \rightarrow \mathbb{R}^n$ is an unconstrained MLP and Π_M is the manifold retraction (Section 5). Given M_s samples $\mathbf{r}^{(m)} \sim \mathcal{P}_{\text{base}}$ and K adversarial test functions $\{f^{(k)}\}$, the empirical estimator is

$$\hat{E}^{(k)} = \frac{1}{M_s} \sum_{m=1}^{M_s} \mathcal{L}_{\text{ss}} f^{(k)}(F_\vartheta(\mathbf{r}^{(m)})). \quad (10)$$

The adversarial training objective is the min-max problem:

$$\min_{\vartheta} \max_{\{\boldsymbol{\eta}^{(k)}\}} \frac{1}{K} \sum_{k=1}^K (\hat{E}^{(k)})^2, \quad (11)$$

where $\boldsymbol{\eta}^{(k)} = \{\mathbf{w}^{(k)}, b^{(k)}\}$ are the test-function parameters defined in Section 4.

4 Ambient Plane-Wave Test Functions

4.1 Definition

Following the flat-space WANPF [1], the test functions are ambient plane waves:

$$f^{(k)}(x) = \sin(\mathbf{w}^{(k)} \cdot x + b^{(k)}), \quad k = 1, \dots, K, \quad (12)$$

with learnable parameters $\mathbf{w}^{(k)} \in \mathbb{R}^n$ and $b^{(k)} \in \mathbb{R}$. For the time-dependent case an additional temporal phase $\kappa^{(k)}t$ is included (Section 6).

4.2 Laplace–Beltrami Action on Plane Waves

Setting $\phi^{(k)} := \mathbf{w}^{(k)} \cdot \mathbf{x} + b^{(k)}$, the ambient Euclidean derivatives are $\nabla f^{(k)} = \cos(\phi^{(k)}) \mathbf{w}^{(k)}$ and $\nabla^2 f^{(k)} = -\sin(\phi^{(k)}) \mathbf{w}^{(k)} (\mathbf{w}^{(k)})^\top$. Substituting into (4) gives the key formula:

$$\boxed{\Delta_g f^{(k)}|_M = -\sin(\phi^{(k)}) (\mathbf{w}^{(k)})^\top P(x) \mathbf{w}^{(k)} - \cos(\phi^{(k)}) H(x) \cdot \mathbf{w}^{(k)}}. \quad (13)$$

The first term involves the *projected squared frequency* $|\mathbf{w}|_P^2 := \mathbf{w}^\top P(x) \mathbf{w}$, and the second is a curvature correction proportional to $H(x) \cdot \mathbf{w}$. Both are computable without automatic differentiation once $P(x)$ and $H(x)$ are known for the specific manifold.

Remark 4.1 (Flat-space recovery). *For $M = \mathbb{R}^n$ one has $P = I_n$ and $H = 0$, so $\Delta_g f^{(k)} = -|\mathbf{w}^{(k)}|^2 \sin \phi^{(k)}$, recovering the standard WANPF formula [1].*

Remark 4.2 (Non-eigenfunction character). *Unlike in flat space, plane waves are not eigenfunctions of Δ_g on a curved manifold: the curvature correction introduces a $\cos \phi$ term that mixes phases. Nevertheless, as adversarially optimized test probes, they remain effective.*

Using (13) and the tangential drift formula $\langle \mathbf{b}(x), \nabla_g f^{(k)}(x) \rangle_g = \cos(\phi^{(k)}) \langle P(x) \mathbf{b}(x), \mathbf{w}^{(k)} \rangle$, the backward Kolmogorov operator on a steady-state plane wave evaluates to:

$$\begin{aligned} \mathcal{L}_{\text{ss}} f^{(k)}(x) &= -\frac{\sigma^2}{2} \sin(\phi^{(k)}) (\mathbf{w}^{(k)})^\top P(x) \mathbf{w}^{(k)} \\ &\quad - \frac{\sigma^2}{2} \cos(\phi^{(k)}) H(x) \cdot \mathbf{w}^{(k)} \\ &\quad + \cos(\phi^{(k)}) \langle P(x) \mathbf{b}(x), \mathbf{w}^{(k)} \rangle. \end{aligned} \quad (14)$$

All three terms are closed-form at each sample on M .

5 Manifold-Constrained Pushforward Architecture

5.1 Retraction-Based Generator

The pushforward map must satisfy $F_{\mathfrak{g}}(t, \mathbf{x}_0, \mathbf{r}) \in M$ for all arguments. We achieve this by composing an unconstrained residual network $\tilde{F}_{\mathfrak{g}} : \mathbb{R}^{1+n+d} \rightarrow \mathbb{R}^n$ with a manifold retraction Π_M :

$$F_{\mathfrak{g}}(t, \mathbf{x}_0, \mathbf{r}) = \Pi_M \left(\mathbf{x}_0 + \sqrt{t} \tilde{F}_{\mathfrak{g}}(t, \mathbf{x}_0, \mathbf{r}) \right). \quad (15)$$

Here $\mathbf{x}_0 \sim \rho_0$ is an initial sample on M and $\mathbf{r} \sim \mathcal{P}_{\text{base}}$ is a d -dimensional noise vector. The \sqrt{t} prefactor ensures that $F_{\mathfrak{g}}(0, \mathbf{x}_0, \mathbf{r}) = \Pi_M(\mathbf{x}_0) = \mathbf{x}_0$ since $\mathbf{x}_0 \in M$ already, so the initial condition $\rho(0, \cdot) = \rho_0$ is satisfied automatically.

For commonly encountered manifolds the retraction Π_M has an analytical form:

- **Sphere** S^{n-1} : $\Pi_M(\mathbf{v}) = \mathbf{v} / \|\mathbf{v}\|$.
- **Stiefel manifold** $\text{St}(n, k)$: polar retraction $\Pi(\mathbf{V}) = \mathbf{V}(\mathbf{V}^\top \mathbf{V})^{-1/2}$.
- **Flat torus** \mathbb{T}^n : componentwise wrapping $\Pi(\mathbf{v}) = (\cos v_i, \sin v_i)_{i=1}^n$.

Remark 5.1 (Parametrization alternative). When M admits a global chart $\psi : \mathbb{R}^m \rightarrow M$ (e.g., stereographic projection for S^{n-1} , or the exponential map for Lie groups), one can instead define $F_{\vartheta} := \psi(\xi_{\vartheta})$ where ξ_{ϑ} is a network in the parameter space \mathbb{R}^m . This avoids the projection step but introduces chart singularities for most manifolds of interest; the retraction approach (15) is therefore preferred.

5.2 Network Specification

For the sphere experiments in Section 8 we use a *steady-state* generator (no t or \mathbf{x}_0 argument):

$$F_{\vartheta}(\mathbf{r}) = \frac{\tilde{F}_{\vartheta}(\mathbf{r})}{\|\tilde{F}_{\vartheta}(\mathbf{r})\|}, \quad \tilde{F}_{\vartheta} : \mathbb{R}^d \xrightarrow{\text{MLP}} \mathbb{R}^3, \quad (16)$$

with tanh activations throughout. The network dimensions and training hyperparameters are listed in Table 1.

6 Time-Dependent WANPF on a Manifold

6.1 Weak Formulation

Let $f \in C^\infty([0, T] \times M)$ be a smooth test function. Multiplying the time-dependent FPE (1) by f , integrating over $M \times [0, T]$, and integrating by parts in both time and space (boundary terms vanish by compactness) gives:

$$\begin{aligned} \int_M f(T, x) \rho(T, x) \, d\text{Vol}_g - \int_M f(0, x) \rho_0(x) \, d\text{Vol}_g \\ - \int_0^T \int_M \rho(t, x) \left(\partial_t f + \frac{\sigma^2}{2} \Delta_g f + \mathbf{b}(f) \right) \, d\text{Vol}_g \, dt = 0. \end{aligned} \quad (17)$$

Since the pushed-forward samples $\mathbf{x}(t) = F_{\vartheta}(t, \mathbf{x}_0, \mathbf{r})$ are distributed according to $\rho(t, \cdot)$ when ϑ is correct, the identity (17) becomes three Monte Carlo estimable terms:

$$\hat{E}_T^{(k)} - \hat{E}_0^{(k)} - \hat{E}^{(k)} = 0, \quad (18)$$

with the time-dependent plane-wave test functions:

$$f^{(k)}(t, x) = \sin(\mathbf{w}^{(k)} \cdot x + \kappa^{(k)} t + b^{(k)}), \quad (19)$$

where $\kappa^{(k)} \in \mathbb{R}$ is a learnable temporal frequency.

6.2 Monte Carlo Estimators

Let $\phi^{(k)} := \mathbf{w}^{(k)} \cdot x + \kappa^{(k)} t + b^{(k)}$. The three estimators in (18) are:

Terminal term. Draw M_T samples $\mathbf{x}_{0,T}^{(m)} \sim \rho_0$ and $\mathbf{r}_T^{(m)} \sim \mathcal{P}_{\text{base}}$:

$$\hat{E}_T^{(k)} = \frac{1}{M_T} \sum_{m=1}^{M_T} f^{(k)}\left(T, F_{\vartheta}(T, \mathbf{x}_{0,T}^{(m)}, \mathbf{r}_T^{(m)})\right). \quad (20)$$

Initial term. Draw M_0 samples $\mathbf{x}_0^{(m)} \sim \rho_0$ directly:

$$\hat{E}_0^{(k)} = \frac{1}{M_0} \sum_{m=1}^{M_0} f^{(k)}(0, \mathbf{x}_0^{(m)}). \quad (21)$$

Interior term. Draw M triples $t^{(m)} \sim \mathcal{U}(0, T)$, $\mathbf{x}_0^{(m)} \sim \rho_0$, $\mathbf{r}^{(m)} \sim \mathcal{P}_{\text{base}}$, and set $\mathbf{x}^{(m)} = F_{\boldsymbol{\vartheta}}(t^{(m)}, \mathbf{x}_0^{(m)}, \mathbf{r}^{(m)})$:

$$\hat{E}^{(k)} = \frac{T}{M} \sum_{m=1}^M \left[\kappa^{(k)} \cos(\phi^{(k)}) + \frac{\sigma^2}{2} \Delta_g f^{(k)} + \cos(\phi^{(k)}) \langle P(x) \mathbf{b}(x), \mathbf{w}^{(k)} \rangle \right]_{(t^{(m)}, \mathbf{x}^{(m)})}, \quad (22)$$

where $\Delta_g f^{(k)}$ is evaluated via (13).

6.3 Adversarial Training Objective

The total loss aggregates the squared residuals over all K test functions:

$$\mathcal{L}_{\text{total}}[\boldsymbol{\vartheta}, \{\boldsymbol{\eta}^{(k)}\}] = \frac{1}{K} \sum_{k=1}^K (\hat{E}_T^{(k)} - \hat{E}_0^{(k)} - \hat{E}^{(k)})^2, \quad (23)$$

with $\boldsymbol{\eta}^{(k)} = \{\mathbf{w}^{(k)}, \kappa^{(k)}, b^{(k)}\}$. Training follows the min-max scheme:

$$\min_{\boldsymbol{\vartheta}} \max_{\{\boldsymbol{\eta}^{(k)}\}} \mathcal{L}_{\text{total}}. \quad (24)$$

The generator (minimiser) and test-function network (maximiser) are updated with separate Adam optimisers, with gradient ascent for the adversary and gradient descent (with gradient clipping) for the generator.

7 Explicit Formulae for Key Manifolds

We record the projection matrix $P(x)$, the mean-curvature vector $H(x)$, and the resulting Laplace–Beltrami formula (13) for the two manifolds most frequently encountered in applications.

7.1 The Unit Sphere $S^{n-1} \subset \mathbb{R}^n$

For $x \in S^{n-1}$ (i.e. $\|x\| = 1$), the tangential projection and mean-curvature vector are:

$$P(x) = I_n - xx^\top, \quad H(x) = -(n-1)x. \quad (25)$$

Substituting into (13) gives:

$$\begin{aligned} \Delta_g f^{(k)}|_{S^{n-1}} &= -\sin(\phi^{(k)}) (|\mathbf{w}^{(k)}|^2 - (x \cdot \mathbf{w}^{(k)})^2) \\ &\quad + (n-1) \cos(\phi^{(k)}) (x \cdot \mathbf{w}^{(k)}). \end{aligned} \quad (26)$$

For $S^2 \subset \mathbb{R}^3$ (i.e. $n = 3$) the constant factor is $n - 1 = 2$.

7.2 The Flat Torus $\mathbb{T}^n \subset \mathbb{R}^{2n}$

Embed the n -torus as $M = \{(\cos \theta_i, \sin \theta_i)_{i=1}^n\} \subset \mathbb{R}^{2n}$. The tangent space is spanned by the n vectors $e_i = (0, \dots, -\sin \theta_i, \cos \theta_i, \dots, 0)^\top$, and the mean-curvature vector vanishes because each factor is a unit circle: $H(x) = 0$. Writing $\mathbf{w} = (w_1^c, w_1^s, \dots, w_n^c, w_n^s)^\top \in \mathbb{R}^{2n}$, the projected squared frequency is:

$$\mathbf{w}^\top P(x) \mathbf{w} = \sum_{i=1}^n (-w_i^c \sin \theta_i + w_i^s \cos \theta_i)^2, \quad (27)$$

and therefore $\Delta_g f^{(k)} = -\sin(\phi^{(k)}) \mathbf{w}^\top P(x) \mathbf{w}$, with no curvature correction.

8 Numerical Experiment: Double-Well FPE on S^2

8.1 Problem Setup

We consider the steady-state Fokker–Planck equation (5) on the unit sphere $S^2 \subset \mathbb{R}^3$ with diffusion coefficient $\sigma = 0.5$ and potential-derived drift $\mathbf{b}(x) = -P(x)\nabla V(x)$. The potential is a double-well function on \mathbb{R}^3 restricted to S^2 :

$$V(x, y, z) = \alpha(x^2 - 1)^2 + \beta z^2, \quad \alpha = 4.0, \beta = 2.0. \quad (28)$$

The two wells of V are located at $(\pm 1, 0, 0)$ on S^2 , where $V = 0$. The βz^2 term confines mass to the equatorial band and prevents the distribution from spreading toward the poles. Figure 1 shows the potential V in longitude–latitude coordinates.

The Gibbs invariant measure is $\rho_\infty(x) \propto e^{-2V(x)/\sigma^2}$, which concentrates sharply near $(\pm 1, 0, 0)$ for the chosen parameters.

8.2 Ambient Gradient and Drift

The Euclidean gradient of V is:

$$\nabla V(x, y, z) = (4\alpha(x^2 - 1)x, 0, 2\beta z)^\top. \quad (29)$$

The manifold drift $\mathbf{b}(x) = -P(x)\nabla V(x)$ is then obtained by projecting $-\nabla V$ onto the tangent plane of S^2 at x , using $P(x) = I_3 - xx^\top$.

8.3 Architecture and Training

The generator is a two-layer MLP with width 32 and tanh activations, mapping a $d = 3$ -dimensional standard Gaussian base distribution $\mathbf{r} \sim \mathcal{N}(0, I_3)$ to S^2 via normalization:

$$F_\vartheta(\mathbf{r}) = \frac{\tilde{F}_\vartheta(\mathbf{r})}{\|\tilde{F}_\vartheta(\mathbf{r})\|}. \quad (30)$$

The adversarial test functions are $K = 200$ ambient plane waves (12) with parameters initialized as $\mathbf{w}^{(k)} \sim \mathcal{N}(0, 4I_3)$ and $b^{(k)} \sim \mathcal{N}(0, 0.25)$. The $\mathcal{L}_{\text{ss}} f^{(k)}(x)$ evaluator uses the

Table 1: Hyperparameters for the S^2 double-well experiment.

Parameter	Symbol	Value
Diffusion coefficient	σ	0.5
Base dimension	d	3
Generator hidden width	—	32
Generator depth	—	2 layers
Number of test functions	K	200
Monte Carlo batch size	M_s	200
Training steps	N	5,000
Generator learning rate	η_{θ}	10^{-3} (cosine annealing)
Adversary learning rate	η_{η}	5×10^{-3}
Potential parameters	α, β	4.0, 2.0

closed-form formula (14) specialized to S^2 via (26), with no automatic differentiation through the geometry. Training hyperparameters are summarized in Table 1.

The training loop alternates one adversary gradient-ascent step (maximizing the loss over $\{\boldsymbol{\eta}^{(k)}\}$) with one generator gradient-descent step (minimizing the loss over $\boldsymbol{\vartheta}$), with gradient clipping of norm 1.0 applied to the generator. A cosine annealing schedule is applied to the generator learning rate from 10^{-3} down to 10^{-5} over the 5,000 steps.

8.4 Results

Figure 1 shows the double-well potential V on S^2 in a longitude–latitude (Plate Carrée) projection alongside the histogram of learned sample density produced by the trained generator.

Figure 2 shows additional diagnostics: the adversarial training loss on a log scale, the pushed-forward samples on the sphere coloured by the x -coordinate, and a Mollweide projection of the samples.

The key qualitative observations are as follows. The learned distribution concentrates mass near both well bottoms at $(\pm 1, 0, 0)$ and is strongly suppressed near the poles, as expected from the βz^2 confinement term in V . The approximate symmetry between the two wells is preserved, reflecting the $x \rightarrow -x$ symmetry of V . The training loss converges to a stationary level after approximately 2,000 steps, with subsequent fluctuations characteristic of the min-max adversarial dynamics.

9 Discussion

9.1 Advantages of the Manifold Formulation

The manifold WANPF inherits all structural advantages of the flat-space method [1]: samples are generated rather than a pointwise density, so probability conservation is exact; the weak formulation requires no mesh, no chart atlas, and no Jacobian determinant; and the method handles multimodal distributions without any explicit mixture structure.

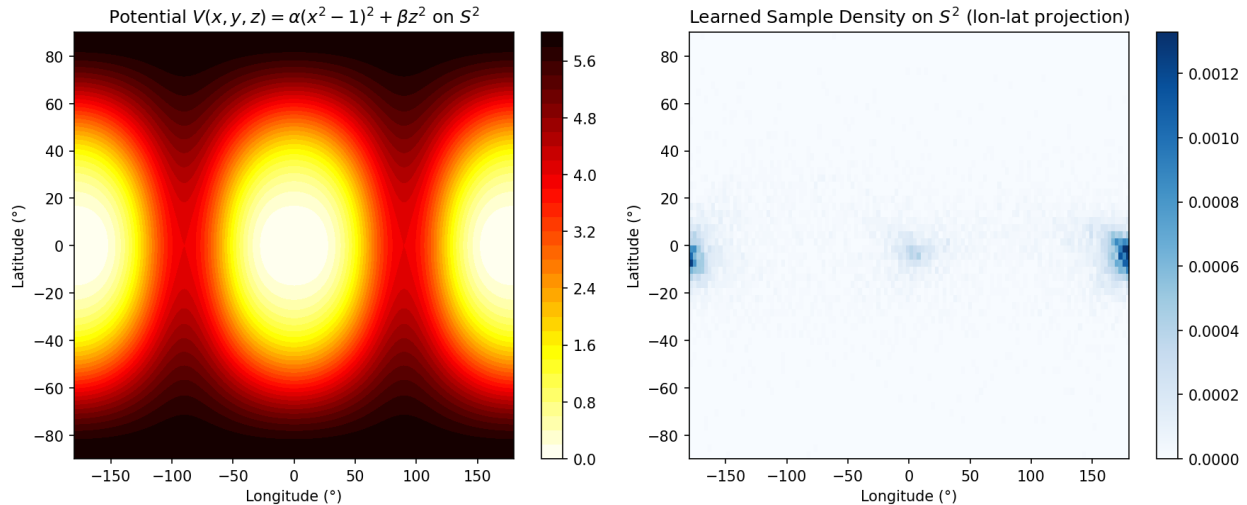


Figure 1: Left: the double-well potential $V(x, y, z) = \alpha(x^2 - 1)^2 + \beta z^2$ on S^2 , shown in longitude–latitude projection. The two potential minima ($V = 0$) are located at longitude 0° and $\pm 180^\circ$ on the equator, corresponding to $(\pm 1, 0, 0)$. Right: density histogram of 8,000 samples generated by the trained neural pushforward map in the same coordinate system. Mass concentrates near both well bottoms and is absent near the poles, consistent with the Gibbs distribution $\rho_\infty \propto e^{-2V/\sigma^2}$ for $\sigma = 0.5$.

The manifold extension adds two further benefits. First, the retraction architecture $F_\vartheta = \Pi_M \circ \tilde{F}_\vartheta$ keeps all samples on M at no additional training cost beyond a single projection per forward pass. Second, the closed-form Laplace–Beltrami formula (13) bypasses all automatic differentiation through the geometry of M , making the per-step cost independent of the number of layers in the intrinsic differential operators.

9.2 Connection to Geometric Measure Theory

The use of ambient test functions is consistent with the theory of varifolds, where the key identity

$$\int_M \rho \Delta_g f \, d\text{Vol}_g = \int_M \rho (\nabla^2 f : P - \nabla f \cdot H) \, d\text{Vol}_g \quad (31)$$

expresses the Laplace–Beltrami action entirely through ambient quantities evaluated on samples in \mathbb{R}^n [5]. WANPF exploits precisely this identity.

9.3 Extension to Non-Isotropic Diffusion

The derivation extends directly to the general FPE with a diffusion tensor a (a positive-definite $(2, 0)$ -tensor on M). The backward Kolmogorov operator becomes $\mathcal{L}f = \frac{1}{2} \text{div}_g(a(df)) + \mathbf{b}(f)$, and in ambient coordinates:

$$\mathcal{L}f = \frac{1}{2} \nabla^2 f : PAP^\top - \frac{1}{2} (AP^\top \nabla f) \cdot H + \langle P\mathbf{b}, P\nabla f \rangle, \quad (32)$$

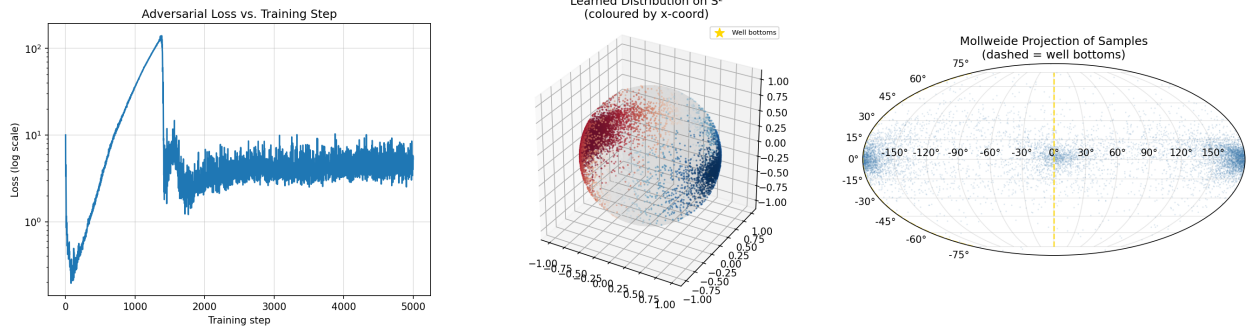


Figure 2: Training and sampling diagnostics for the S^2 double-well experiment. Left: adversarial loss versus training step (log scale). The loss rises during early generator exploration and then decreases as training converges to a stationary min-max point near step 2,000. Center: 8,000 generated samples on S^2 , coloured by their x -coordinate value (red near $x = +1$, blue near $x = -1$); gold stars mark the two well bottoms ($\pm 1, 0, 0$). The generator correctly concentrates mass around both minima symmetrically. Right: Mollweide equal-area projection of the same samples; dashed gold lines indicate the longitudes of the well bottoms. Samples cluster near 0° and $\pm 180^\circ$ longitude, confirming two-well capture, with near-uniform spreading in longitude about each minimum and strong equatorial confinement consistent with the βz^2 term.

where $A \in \mathbb{R}^{n \times n}$ is any ambient extension of a . For the isotropic case $a = \sigma^2 g^{-1}$, $PAP^\top = \sigma^2 P$ and (32) reduces to (14).

9.4 Supplementing with Spherical Harmonics

As noted in Remark 4.2, ambient plane waves are not eigenfunctions of Δ_g on a curved manifold. For S^{n-1} , one could supplement the plane-wave test-function class with spherical harmonics Y_ℓ^m , which *are* eigenfunctions with eigenvalue $-\ell(\ell + n - 2)$. In the WANPF framework this amounts to adding additional test functions whose operator evaluations are analytically known; the min-max training structure is unchanged. We leave a systematic comparison to future work.

9.5 Future Directions

Several extensions are natural. The time-dependent formulation (Section 6) is directly applicable to the heat equation on S^{n-1} or on a Lie group such as $\text{SO}(3)$; the only change is the specification of $P(x)$ and $H(x)$ for the new manifold. For the fractional Fokker–Planck equation on a manifold, one would need to replace the Laplace–Beltrami operator with the spectral fractional Laplacian $(-\Delta_g)^{\alpha/2}$, whose plane-wave action on curved manifolds is no longer as clean but could be approximated via Monte Carlo integration over manifold heat kernels. Higher-dimensional manifolds (e.g., S^{n-1} with $n \geq 10$) are a natural stress test for the mesh-free approach.

10 Conclusion

We have extended the Weak Adversarial Neural Pushforward Method to the Fokker–Planck equation on compact embedded Riemannian manifolds. The extension rests on three pillars: (i) a retraction-based pushforward architecture that keeps samples on M by construction; (ii) ambient plane-wave test functions whose Laplace–Beltrami operators are computable in closed form via the tangential projection $P(x)$ and mean-curvature vector $H(x)$; and (iii) a min-max adversarial loss whose Monte Carlo estimator requires only pointwise evaluations at samples on M , with no mesh, no chart, and no Jacobian computation.

The resulting algorithm for the steady-state case is summarized in Algorithm 1. Numerical experiments on the double-well FPE on S^2 confirm that the trained generator correctly concentrates mass near both potential minima, consistent with the Gibbs invariant measure.

Algorithm 1 Steady-State Manifold WANPF

Require: manifold M with retraction Π_M , $P(\cdot)$, $H(\cdot)$; drift \mathbf{b} ; diffusion σ ; learning rates η_ϑ , η_η ; batch size M_s ; steps N .

- 1: Initialize generator F_ϑ and test-function parameters $\{\boldsymbol{\eta}^{(k)}\}_{k=1}^K$.
- 2: **for** step = 1, \dots , N **do**
- 3: **Adversary step:** sample $\{\mathbf{r}^{(m)}\}$, compute $\mathbf{x}^{(m)} = F_\vartheta(\mathbf{r}^{(m)}) \in M$, evaluate $\hat{E}^{(k)}$ via (10) and (14), update $\boldsymbol{\eta}^{(k)} += \eta_\eta \nabla_{\boldsymbol{\eta}} \mathcal{L}$ (gradient ascent).
- 4: **Generator step:** same forward pass, update $\vartheta -= \eta_\vartheta \nabla_{\vartheta} \mathcal{L}$ (gradient descent).
- 5: **end for**

Ensure: generator F_ϑ approximating the invariant measure ρ_∞ .

The framework is directly applicable to any manifold for which $P(x)$ and $H(x)$ can be computed analytically or numerically, and it scales to dimensions inaccessible by mesh-based solvers.

References

- [1] A. Q. He and W. Cai, Neural Pushforward Samplers for Transient Distributions from Fokker–Planck Equations with Weak Adversarial Training, *arXiv:2509.14575*, 2025.
- [2] E. P. Hsu, *Stochastic Analysis on Manifolds*, Graduate Studies in Mathematics, vol. 38. American Mathematical Society, Providence, RI, 2002.
- [3] M. Girolami and B. Calderhead, Riemann manifold Langevin and Hamiltonian Monte Carlo methods, *Journal of the Royal Statistical Society: Series B*, 73(2):123–214, 2011.
- [4] N. Lei, K. Su, L. Cui, S.-T. Yau, and D. X. Gu, A geometric view of optimal transportation and generative model, *Computer Aided Geometric Design*, 78:101851, 2020.
- [5] L. Simon, *Lectures on Geometric Measure Theory*, Proceedings of the Centre for Mathematical Analysis, vol. 3. Australian National University, Canberra, 1983.

- [6] Y. Zang, G. Bao, X. Ye, and H. Zhou, Weak adversarial networks for high-dimensional partial differential equations, *Journal of Computational Physics*, 411:109409, 2020.
- [7] M. Raissi, P. Perdikaris, and G. E. Karniadakis, Physics-informed neural networks: A deep learning framework for solving forward and inverse problems involving nonlinear partial differential equations, *Journal of Computational Physics*, 378:686–707, 2019.
- [8] E. Weinan and B. Yu, The deep Ritz method: a deep learning-based numerical algorithm for solving variational problems, *Communications in Mathematics and Statistics*, 6(1):1–12, 2018.